Experimental Analysis of Current and Deformation of Ion-exchange Polymer Metal Composite Actuators

by E.T. Enikov and G.S. Seo

ABSTRACT—In this paper we describe the experimental analysis of a novel ion-exchange polymer metal composite (IPMC) actuator under large external voltage. The experimental analysis is supplemented with a coupled thermodynamic model, which includes mass transport across the thickness of the polymer actuator, chemical reactions at boundaries, and deformation as a function of the solvent (water) distribution. In this paper, the case of large electrode potentials (over 1.2 V) has been analyzed experimentally and theoretically. At these voltage levels, electrochemical reactions take place at both electrodes. These are used in the framework of overpotential theory to develop boundary conditions for the water transport in the bulk of polymer. The model is then simplified to a three-component system comprised of a fixed negatively charged polymeric matrix, protons, and free water molecules within the polymer matrix. Among these species, water molecules are considered to be the dominant species responsible for the deformation of the IPMC actuators. Experiments conducted at different initial water contents are described and discussed in the context of the proposed deformation mechanism. Comparison of numerical simulations with experimental data shows good agreement.

KEY WORDS—IPMC actuators, fuel cell, overpotential theory, water transport, swelling

Introduction

Ion-exchange membranes are used in applications ranging from hydrogen fuel cells to the production of sodium or potassium hydroxide (ion separation). When structured as metal–polymer–metal composite sheets, they can also operate as actuators called ion-exchange polymer metal composite (IPMC) actuators. The structure of this type of actuator, shown in Fig. 1(a), consists of an ion-exchange polymer matrix sandwiched between two metal electrodes. The reader is referred to an excellent review article[1] on the chemical and micromorphological properties of the ion-exchange polymer (Nafion^{TM}) used in this work.

IPMC actuators can be produced by an electrochemical platinization method based on the ion-exchange properties of the polymer.[2] The method consists of two main steps: (i) ion exchange of the protons H^+ with metal cations (Pt^{2+}); (ii) chemical reduction of the metal ions onto the membrane surface with $NaBH_4$. IPMC actuators used in this work are Nafion^{TM}–platinum composites produced by this process following the detailed protocol from Oguro.[3] The protocol results in an H^+ form of IPMC, produced by soaking the material in diluted hydrochloric acid. The H^+ cations were not exchanged for other cations, as is commonly done by others[4–6], in order to be able to use the proton mobility data developed independently by other groups. Figure 2 shows a scanning electron microphotograph of the fabricated composite. The right photograph shows the Pt particles (white phase) at the boundary, indicating that the electrode surface is approximately 0.8 μm thick.

When an external potential is applied between points A and B (Fig. 1(b)), the cations in the bulk of the polymer migrate towards the cathode, carrying along water molecules. The volume associated with these water molecules causes local matrix expansion, resulting in deformation of the composite. This view of the underlying mechanism is a subject of debate as various research groups have suggested slightly different deformation models in an effort to adequately describe the actuator. To date, most work has been done in the low-voltage regime (below the 1.2 V equilibrium potential of Pt), and the reason for this is that electrochemical reactions produce gas at high voltages. If encapsulated, these actuators will have packaging problems. Therefore, attempts have been made to operate the actuators under low potentials. To compensate for the greatly reduced displacement, many have tried to replace the migrating ion with a large counter ions, or ions with large hydration shells.[4–6] Applying higher voltage, however, will always produce larger deformation and in many applications (e.g., a deformable catheter or underwater swimming robot[7,8]) the actuators can be in direct contact with the electrolyte solution. In these cases, the liberated gas does not pose significant limitations. Under these conditions, which are the subject of this paper, ionic transport, water back-diffusion, and concentration gradients have to be considered in the deformation process responsible for the bending of the composite.

Shahinpoor[9] proposed one of the first models based on the large deformation theory of ionic polymeric gels in an electric field and a pH gradient. This model considers the effect of the internal electric charge redistribution of fixed and mobile ions due to the presence of the electric field, and describes a purely electrostatic process. Later, Shahinpoor[10] presented a Euler–Bernoulli beam model of a non-homogeneously distributed electrically induced moment. The moment was attributed to the presence of a non-homogeneous electric field in the elastic material. Kanno et al.[11] presented a lumped parameter linear model of the ionic polymer actuator, where the step response

E.T. Enikov (SEM member; enikov@engr.arizona.edu) is an Assistant Professor and G.S. Seo is a Research Associate, Department of Aerospace and Mechanical Engineering, University of Arizona, Tucson, AZ 85721, USA.

Original manuscript submitted: January 25, 2005.
Final manuscript received: April 29, 2005.
DOI: 10.1177/0014485105056091

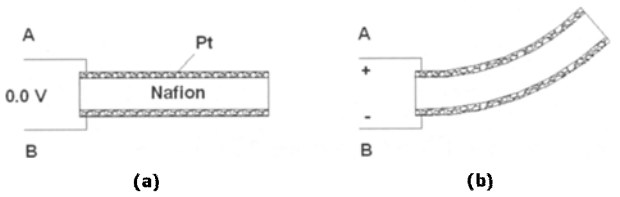

Fig. 1. Polymer/metal composite actuator

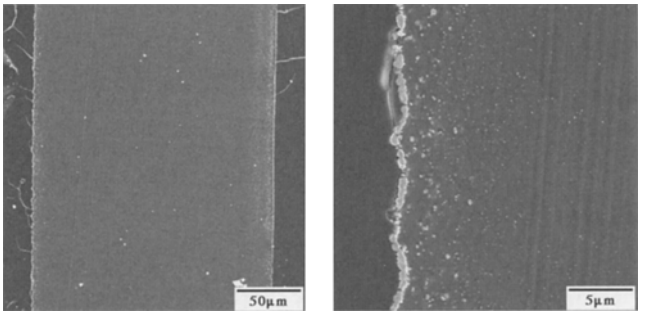

Fig. 2. Nafion™ membrane with Pt electrodes on each side (white regions are Pt particles of the electrodes)

of the actuator was empirically modeled as a linear dynamical system with two real poles. Kanno et al.[12] proposed a gray-box model. In their model, the ionic polymer was modeled as a network of a capacitor and resistor in series. A higher-order lumped parameter model was presented by Bao et al.[13]. They suggested two subsystems: a distributed RC line model to describe the "varying capacitance" of the electric input behavior, and a four-lumped parameter system to express the relaxation phenomena. These models were constructed based on experimental observations rather than on the analysis of the microphysiochemical processes.

The first comprehensive microscopic treatment was presented by Nemat-Nasser and Li.[5] Their model considered the microstructure of a water-saturated ionic polymer–metal composite in air, and explained the observed rapid (of the order of a few seconds) response with the internal stresses produced by the redistribution of the cations locally, near the surface of the two electrodes. Later, Nemat-Nasser[14] modified this model, and explained the quick and small-amplitude response to a suddenly applied electric field using the electrostatic forces arising in a thin region near the electrodes where an imbalanced net charge exists. In his model, under an externally applied electric potential below the 1.2 V equilibrium potential, the cations are redistributed locally. In the resulting anion-rich region, the polymer chains relax and, in the cation-rich region, they further extend, leading to relatively small bending (0.08 mm mm^{-1}) of the polymer membrane. In order to reproduce his experimental observations, parameters such as the cluster size, a, the polymer relaxation times, τ and τ_1, and hydraulic permeability coefficient, D_a, were chosen "somewhat arbitrarily to yield reasonable results".[14] In contrast, at higher potentials (exceeding the equilibrium potential of 1.2 V for Pt) the specific deformation reaches 0.4 mm^{-1}, even with relatively small counter ions such as protons. Further, the current transients occur with time constants exceeding 100 s, which is two orders of magnitude larger than the time constants observed at lower external potentials. If the electrostatic model proposed in Nemat-Nasser[14] were to be adopted for this voltage regime, it would be impossible to explain the long-lived current and deformation transients with processes occurring at the anodes alone.

The objective of this work is to propose and evaluate the feasibility of an alternative deformation model based on the solvent (water) being the main factor responsible for the observed deformation under the higher potential regime. In this paper we follow an indirect approach, which uses water and proton transport data derived by independent research groups and compares the predicted deformation with the experimental observations made by the authors. In doing so, we hope to provide indirect evidence on the central role of the solvent in the deformation process, which is also consistent with the body of research on polymer-based fuel cells.

Transport Model and Chemical Reactions

The actuator model includes mass transport within the membrane, reactions at the boundaries, and deformation (strain) induced by a water concentration gradient. Figure 3(a) is a schematic diagram of the ionic transport processes taking place inside the polymer. This model is commonly used in hydrogen–oxygen fuel cells.[15] When an external potential is applied between the two electrodes, water molecules dissociate, producing protons, electrons, and oxygen gas at the anodic side. While oxygen gas and hydrogen gas are released at the anode and cathode,[16] respectively, the external electric field generates a flux of protons towards the cathode. In the process, water molecules are carried by proton drag towards the cathode. At the cathode, these protons pick up an electron and produce hydrogen gas. As a result, the concentration of water molecules near the anode is reduced, and water is accumulated near the cathode. Due to the redistribution of water within the membrane, the polymer network matrix near the cathode expands and that near the anode contracts, resulting in initial net bending towards the anodic side. Associated with this are the gradients of water concentration and polymer strain. These gradients generate a flux of water molecules in the opposite direction, governed by a law that is macroscopically similar to Darcy's law for pressure-driven flow in porous media.[17] Due to these water fluxes, the distribution of water changes. As a result, the gradient of water concentration is reduced and the actuator gradually back relaxes towards the cathode.

These molar fluxes can be described using the Onsager theory of thermodynamic fluxes and their driving forces[18]

$$j_i^n = -\sum_s \alpha^{ns}\left(\frac{\mathcal{R}\theta}{\mathcal{M}^s c^s}\nabla_i c^s + \frac{\mathcal{F}z^s}{\mathcal{M}^s}\nabla_i\phi - K\frac{\bar{\mathcal{V}}^s}{\mathcal{M}^s}\nabla_i L_{kk}^{poly}\right), \tag{1}$$

where $\mathcal{R}$ is the gas constant, θ is temperature, $\mathcal{F}$ is the Faraday constant, ϕ is the electric potential, K is the bulk modulus, L_{kk}^{poly} is the elastic strain of polymer network, α^{ns} is the molar mobility coefficient tensor, $\mathcal{M}^s$ is the molar mass, c^s is the molar concentration, z^s is the valence, and $\bar{\mathcal{V}}^s$ is the molar partial volume of species s. Thus, the first term in eq (1) is due to the gradient of the concentration of species s, the second

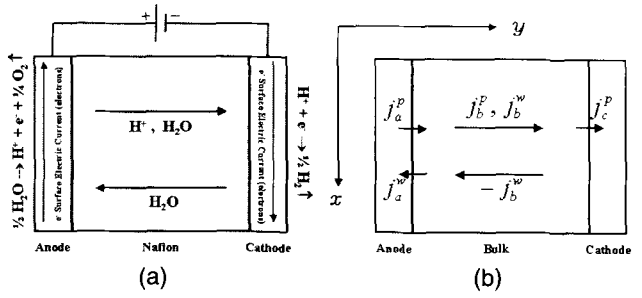

Fig. 3—Transport model (a) and direction of fluxes (b)

term is field driven diffusion, and the last term is due to the gradient of the polymer strain.

In general, at least four species should be considered when modeling the mass transport in the membrane. These are water molecules, protons, hydroxyl ions, and the polymer matrix with covalently bonded perfluorinated sulfonic acid moieties. The negatively charged co-ions (OH^-), however, are in low concentration, since they are introduced from the external solution,[19] which in the current study was deionized water with low ionic content (18 MOhm cm resistivity). Since there are no reactions producing new hydroxyl groups, it is expected that the current due to co-ions is very small. For example, for the current electrode geometry the hydroxyl groups and protons would collectively result in 0.02–0.2 mA current in pure deionized water, which is three to four orders of magnitude smaller than the measured current during the experiment. Therefore, a three-component model is assumed for the IPMC actuators: protons, water molecules, and perfluorinated sulfonic acid moieties. The perfluorinated sulfonic acid moieties are fixed to the polymer network, and the mobile species are protons and water molecules. For the sake of simplicity it is also assumed that these mobile species flow only along the transversal direction between the two electrodes (y direction in Fig. 3(b)). Since protons are the only mobile charged species, electroneutrality in the bulk of the polymer requires that the proton concentration be constant within the bulk of the membrane ($\nabla c^p = 0$). While the partial molar volume of the protons is not known, since no proton concentration variations are allowed, we can assume it to be zero without affecting the simulation results. Water molecules do not carry free charges and therefore the valence of water, z^w, is also zero. With these simplifications, the molar fluxes of protons and water are expressed as

$$\begin{aligned} j_b^p &= -\alpha^{pp}\frac{\mathcal{F}z^p}{\mathcal{M}^p}\nabla\phi - \alpha^{pw} \\ &\quad \left(\frac{\mathcal{R}\theta}{\mathcal{M}^w c^w}\nabla c^w - K\frac{\tilde{\mathcal{V}}^w}{\mathcal{M}^w}\nabla L_{kk}^{poly}\right) \\ &= -\frac{\sigma}{\mathcal{F}}\nabla\phi - n_d^{pw}\left(D^w\nabla c^w - \tilde{K}c^w\nabla L_{kk}^{poly}\right), \quad (2) \end{aligned}$$

and

$$\begin{aligned} j_b^w &= -\alpha^{wp}\frac{\mathcal{F}z^p}{\mathcal{M}^p}\nabla\phi - \alpha^{ww} \\ &\quad \left(\frac{\mathcal{R}\theta}{\mathcal{M}^w c^w}\nabla c^w - K\frac{\tilde{\mathcal{V}}^w}{\mathcal{M}^w}\nabla L_{kk}^{poly}\right) \\ &= -n_d^{wp}\frac{\sigma}{\mathcal{F}}\nabla\phi - D^w\nabla c^w + \tilde{K}c^w\nabla L_{kk}^{poly}, \quad (3) \end{aligned}$$

respectively. Here, $\sigma = (\alpha^{pp}\mathcal{F}^2 z^p)/\mathcal{M}^p$ is the proton conductivity coefficient of the membrane; $D^w = (\alpha^{ww}\mathcal{R}\theta)/(\mathcal{M}^w c^w)$ is the diffusion coefficient of water in the membrane; $\tilde{K} = (D^w K\tilde{\mathcal{V}}^w)/(\mathcal{R}\theta)$; and $n_d^{pw} = (\alpha^{pw}\mathcal{R}\theta)/(D^w\mathcal{M}^w c^w) = \alpha^{pw}/\alpha^{ww}$ and $n_d^{wp} = (\alpha^{wp}\mathcal{F}^2 z^p)/(\sigma\mathcal{M}^p) = \alpha^{wp}/\alpha^{pp}$ are the drag coefficients of the proton flux and water flux, respectively. The upper indexes p and w denote protons and water molecules, respectively, and the lower index b denotes the bulk portion of the membrane. The proton flux in the membrane is proportional to the electric field and is affected by the water flux. The first term in eq (3) is due to the drag effect of the protons, the second term is diffusion due to the gradient of concentration, and the last term is due to the gradient of elastic strain.

The molar fluxes at both electrodes are predicted from the overpotential theory. When current flows through a redox electrode, the current–potential relationship depends on the activation overpotential and is expressed as[20]

$$i = k_+ c_r \exp\left(\frac{\alpha\mathcal{F}}{\mathcal{R}\theta}\varepsilon\right) - k_- c_0 \exp\left[-\frac{(1-\alpha)\mathcal{F}}{\mathcal{R}\theta}\varepsilon\right], \quad (4)$$

where i is the current density, ε is the electrode external potential, k_+ is the anodic reaction coefficient, k_- is the cathodic reaction coefficient, c_r is the concentration of reactants, c_0 is the concentration of products, and α is the charge transfer barrier or symmetry coefficient. For higher anodic (positive) overpotentials, the second term in eq (4) becomes negligible, and for higher cathodic (negative) overpotentials, the first term in eq (4) becomes negligible. For the analysis of an actuator, it is assumed that the thickness of a reaction layer is quite small in comparison with the thickness of the actuator, and therefore can be neglected. Further, no electrons and protons are accumulated at the electrodes during deformation. The chemical reaction equations at the anode and cathode are[15]

$$\frac{1}{2}H_2O \rightarrow H^+ + e^- + \frac{1}{4}O_2\uparrow \quad (5)$$

and

$$H^+ + e^- \rightarrow \frac{1}{2}H_2\uparrow. \quad (6)$$

According to eqs (4) and (5), the molar flux of protons and water at the anode are

$$j_a^p = \frac{i_a}{\mathcal{F}} = \frac{k_+}{\mathcal{F}}(c_a^w)^{1/2}\exp\left(\frac{\alpha_a\mathcal{F}}{\mathcal{R}\theta}\varepsilon_a\right) \quad (7)$$

and

$$j_a^w = -\frac{j_a^p}{2}, \quad (8)$$

respectively, where the lower index a denotes anode and c_a^w is the concentration of water at the anode surface and varies in time. Similarly, the molar fluxes of proton and water at the cathode are

$$j_c^p = \frac{i_c}{\mathcal{F}} = -\frac{k_-}{\mathcal{F}}c_c^p\exp\left[-\frac{(1-\alpha_c)\mathcal{F}}{\mathcal{R}\theta}\varepsilon_c\right] \quad (9)$$

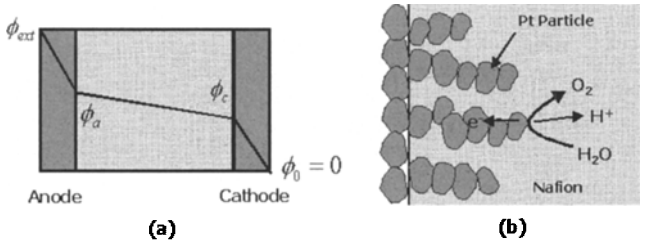

Fig. 4—Distribution of potential (a) and actual area at electrodes (b)

and

$$j_c^w = 0, \tag{10}$$

where the lower index c denotes a cathode and c_c^p is the concentration of proton at the cathode surface. This concentration always remains at its initial value because of the electroneutrality assumption and the charge conservation requirement. Since water molecules are not involved in this chemical reaction, the molar flux of water at the cathode is zero.

Due to charge conservation (except for the initial transient period), the electric current through a closed circuit is constant at all times. The flux of protons in each region has to satisfy the continuity condition as follows

$$j_a^p A_a = j_b^p A_b = j_c^p A_c, \tag{11}$$

where A_a, A_b, and A_c are the actual areas of the anode, bulk, and cathode, respectively. The actual areas of both electrodes are larger than that of the bulk, because these electrodes are porous and a chemical reaction occurs along the entire surface area Pt particles (see Fig. 4 (b)). These areas were determined experimentally by Moore[21] using a hydrogen adsorption and desorption method. Moore's work, which was conducted on electrodes fabricated through a similar process, showed that the area of the platinum electrode is 9.2 times larger than the cross-sectional area of the bulk polymer. In lieu of an ability to repeat these measurements and in accordance with the philosophy of this work, this value has been used to account for the actual surface area. The potential at the outer surface of the cathode is set to zero (the reference potential) and the distribution of the potential in the membrane is assumed linear (Fig. 4 (a)), implying electroneutrality of the bulk of the polymer. This is consistent with the model of Nemat-Nasser[14], which predicts net charge only in the outer 3–6 μm region adjacent to the electrode surface.

Substituting eqs (2), (7), and (9) into eq (11) results in

$$\begin{aligned}
&\frac{\sigma}{\mathcal{F}}\frac{(\phi_a-\phi_c)}{2H} - n_d^{pw}\left(D^w\nabla c^w - \tilde{K}c^w\nabla L_{kk}^{poly}\right)\\
&= \frac{9.2}{\mathcal{F}}k_+(c_a^w)^{1/2}\exp\left[\frac{\alpha_a\mathcal{F}}{R\theta}(\phi_{ext}-\phi_a)\right]\\
&= \frac{9.2}{\mathcal{F}}k_-c_c^p\exp\left[\frac{(1-\alpha_c)\mathcal{F}}{R\theta}\phi_c\right],
\end{aligned} \tag{12}$$

where H is one-half the thickness of actuator and the applied external potential, ϕ_{ext}, is known. The potentials at the inner surface of the anode, ϕ_a, and the potentials at the inner surface of the cathode, ϕ_c, can be solved by the two non-linear implicit equations (12), if the values of the water and proton concentrations are known.

A numerical evaluation the closed system of equations, (3), (8), (10), and (12), along with the conservation of mass

$$\dot{c}_b^w + \nabla j_b^w = 0, \tag{13}$$

representing the entire model, has been performed using the constants and parameters independently measured by other groups (refer to Table 1). From the resulting water concentration gradient predictions, a small-strain, large-displacement solution has been developed as follows. The total deformation of the polymer matrix is decomposed into two additive parts: elastic deformation of the polymer network due to external load and/or electrostatic body forces, L_{ij}^{poly}, and dilatational deformation due to redistribution of ions and solvent, which we call chemical strain and denote by $L_{ij}^{chem} = \sum_s(\bar{\mathcal{V}}^s/3)(c^s - c_0^s)\delta_{ij}$, where $\bar{\mathcal{V}}^s$ are the partial molar volumes and c_0^s are the initial molar concentrations of species s. Since the width of the actuator and the length of the actuator are much longer than its thickness, plane strain can be assumed. Additionally, $L_{xy}^{total} = L_{yy}^{total} = 0$ is also implied due to the Euler–Bernoulli kinematic assumption. The non-zero strain L_{xx}^{total} is then decomposed into average and linearly varying parts as follows

$$L_{xx}^{total} = L_{xx}^{poly} + L_{xx}^{chem} = L_{xx}^{ave} - y\kappa, \tag{14}$$

where κ is the curvature, $L_{xx}^{ave} = \mathrm{d}u(x)/\mathrm{d}x$, and $u(x)$ is the axial displacement of the neutral axis.

Total stress along the axial direction due to the polymer network deformation is

$$T_{xx} = \frac{E}{(1-\nu^2)}L_{xx}^{poly} = \frac{E}{(1-\nu^2)}\left(L_{xx}^{ave} - y\kappa - \frac{\bar{\mathcal{V}}^w}{2}\Delta c^w\right), \tag{15}$$

where $\Delta c^w = c^w(y,t) - c^w(y,0)$. The average strain, L_{xx}^{ave}, and the curvature, κ, are obtained through the two equilibrium conditions implying zero external forces and moments, $\int T_{xx}\mathrm{d}A = 0$ and $\int T_{xx}y\mathrm{d}A = 0$. These results are

$$L_{xx}^{ave} = \frac{\bar{\mathcal{V}}^w}{4H}\int_{-H}^{H}\Delta c^w\mathrm{d}y \tag{16}$$

$$\kappa = \frac{3\bar{\mathcal{V}}^w}{4H^3}\int_{-H}^{H}\Delta c^w y\mathrm{d}y. \tag{17}$$

where H is one-half the thickness of the actuator. Figure 5 shows the displacement of a short beam element. The final shape is obtained by integration of the element rotation angle, $\mathrm{d}\varphi(x_0)$, and the displacement of the beam, $\mathrm{d}X(x_0)$ and $\mathrm{d}Y(x_0)$:

$$\varphi(x_0) = \int_0^{x_0}\kappa(s)\mathrm{d}s \tag{18}$$

$$X(x_0) = \int_0^{x_0}(1 + L_{xx}^{ave})\cos(\varphi(s))\mathrm{d}s \tag{19}$$

TABLE 1—CONSTANTS AND PARAMETERS

Constants/Parameters	Value/Expression	Dimension	Reference
Faraday constant, $\mathcal{F}$	9.6487×10^4	C mol^{-1}	22
Gas constant, R	8.3143	J mol^{-1} K^{-1}	22
Density of dried Nafion™, ρ_m^{dry}	1967	kg m^{-3}	23
Equivalent weight of Nafion™, E_m	1.1	kg mol^{-1}	23
$e = \rho_m^{dry}/E_m$	1788	mol m^{-3}	24
Swelling coefficient, f	0.0126		24
Hydration index, λ	$c^w/(e - fc^w)$		24
Water diffusion coefficient, D^w	$3.5 \times 10^{-6}\lambda \exp(-2436/\theta)$	m^2 s^{-1}	25
Thickness of actuator, $2H$	183	μm	26
Young's modulus of Nafion™ (fully hydrated), E	1.773×10^{11}	Pa	26
Electric conductivity of Nafion™, σ	$(0.5139\ \lambda - 0.326)$		24
Drag coefficient of water flux, n_d^{wp}	$(2.5/22)\ \lambda$		24
Drag coefficient of proton flux, n_d^{pw}	$(n_d^{wp}\sigma R\theta\mathcal{M}^p)/(D^w c^w \mathcal{F}^2 z^p \mathcal{M}^w)$		

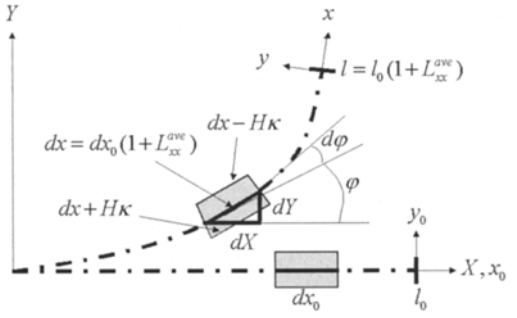

Fig. 5—Beam element before and after deformation, where $x_0 \otimes y_0$ and $x \otimes y$ are the curvilinear coordinates along the neutral axis of initial and deformed shape, and $X \otimes Y$ is the fixed frame.

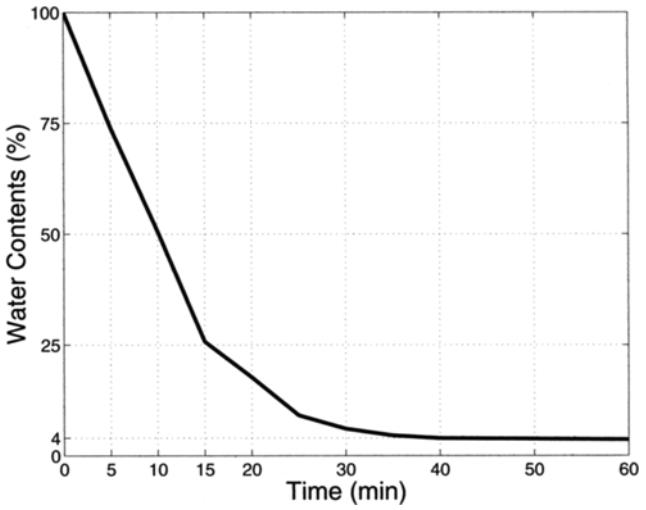

Fig. 6—Initial water contents according to drying time

$$Y(x_0) = \int_0^{x_0} (1 + L_{xx}^{ave}) \sin(\varphi(s))ds. \qquad (20)$$

Actuation Experiments

Several experiments have been performed to evaluate the numerical predictions. To establish the effect of water content on the current and deformation, four samples with different initial water contents were used with 4 V external voltage. Initially, the actuator strips were fully hydrated in deionized water, and then partially dried for 0, 5, 10, and 15 min at room temperature and ambient conditions. The drying curve is shown in Fig. 6. The sample was dried for 60 min at room temperature and ambient conditions replicating the experimental conditions. An additional 12 h long vacuum drying was performed in a vacuum chamber (Labconco, FreeZone 2.5 Plus) at 0.03 mbar and cold trap temperature of −80°C to assess the total water content. This resulted in removal of additional 4% of water content, which was used as reference in developing Fig. 6. Additional points are defined at 74, 51, and 26%, respectively, as established by weight measurements and were used as initial value for the simulations. The fully hydrated samples were subjected to 3, 4, and 5 V, respectively, while the 74, 51, and 26% hydrated samples were subjected to 4 V only.

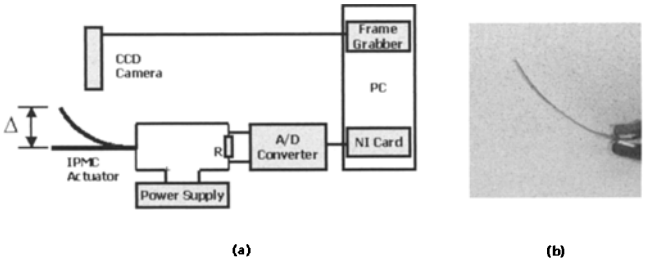

Fig. 7—(a) Schematic diagram of the experimental system and (b) photograph of the deformed actuator

A schematic diagram of the experimental system for the current and displacement measurements is shown in Fig. 7(a). Each experiment was repeated three times, each using three different samples. In each of these, the current and displacement of the actuators were measured simultaneously. The test

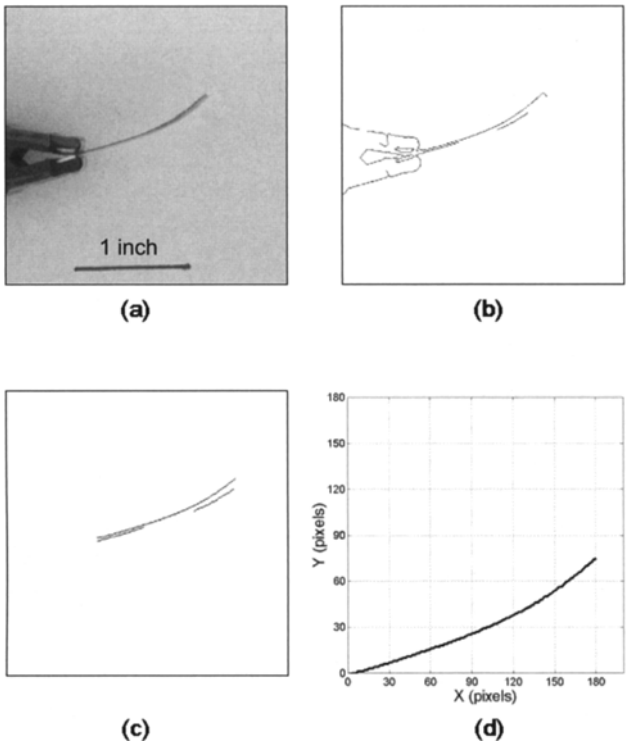

Fig. 8—Image process to calculate the displacement: raw image (a), edge detection (b), IPMC (c), and convert to pixels (d)

samples were 6×30 mm^2 IPMC strips with a thickness of 180 μm. One end of the actuator was fixed by a clamp, and the other end was kept free. To actuate the composite, a constant external voltage was applied between the two platinum electrodes using a power supply (Agilent, 3630A). The current was measured through a 0.5Ω resistor connected in series with the actuator by an A/D converter (NI, PCI 7344). The displacement of the actuator was captured by a CCD camera and a frame grabber (Sensoray, PCI 611). Using an edge detection technique (Canny method), the displacements were calculated. Figure 8 shows one processed image and the results in pixels for one frame captured during the deformation tests.

Discussion of Experimental Results

Figure 9 shows the simulation results for water concentration during the deformation of the IPMC actuator under an external voltage of 4 V. At the beginning, the concentration of water rapidly decreases at the anode and increases at the cathode due to the large proton flux, as dictated by eq (3). This redistribution of water produces a gradient of concentration and internal strain. As a result, a water flux in the opposite direction is generated, and the difference in water concentration between both sides gradually decreases. Eventually the concentration of water at both sides is reduced until complete water depletion is reached. This is due to the water consumption by the chemical reaction at the anode.

The current and displacement history can be predicted through the obtained water concentration evolution. Since the current (proton flux) is proportional to the water concentration at the anode (see eq (7)), the maximum current will occur at the beginning, and then it will decrease gradually over time. This is consistent with the experimental observations shown in Fig. 10(a). Also, according to eq (17) the curvature of the actuator is proportional to the difference of the water concentration between the anode and the cathode. This results in maximal displacement at the beginning of the current transient, followed by a gradual return of the actuator towards its original shape (see Fig. 10(b)).

Figures 11(a) and (b) show simulations of the water concentration evolution of the fully hydrated IPMC actuator under external voltages of 3 and 5 V, respectively. At the higher (5 V) external potential, the water concentration at the anode decreases more rapidly. Since the proton flux is proportional to the external potential, the difference in water concentration between the two sides is also larger for the higher external potential, resulting in larger initial displacement.

Figure 12 shows the numerical results for current history compared to experimental results. The curves represent the numerical results and the symbols show the average measured values from the experiments. The maximum electric current is observed at the beginning, resulting in a large proton flux in the membrane from anode to cathode. Due to the decrease of water molecules at the anode as the result of molar transport and decomposition by the chemical reaction, the current is also decreased accordingly. Eventually, the current reaches a near-zero steady-state value, because almost all of the free water molecules in the membrane are consumed by the chemical reaction. Figure 12(a) illustrates the variation of the current history as a function of the initial water content in the membrane. The maximum value is proportional to the initial water content. The rate of current reduction is also proportional to the initial water content. Since the proton diffusion coefficient is water-dependent,[25] higher water content implies higher current and more rapid transport. Figure 12(b) shows the effect of the externally applied voltages on the current history. As expected, when a higher external voltage is applied between two electrodes, higher anodic and cathodic overpotentials develop at the anode and the cathode. A correspondingly larger current is to be expected, resulting in more rapid decay of the electric current at higher external potentials.

According to the proposed model, the water redistribution in the membrane generates a deformation gradient across the actuator. At the beginning, the large difference in water concentration between both sides produces a large deformation of the actuator towards the anodic side. Subsequently, this difference is gradually reduced due to water flux opposing the gradient of concentration, as well as the gradient of internal pressure. As a result, the actuator slowly deforms toward the cathode and finally returns near its initial position. This is observed in the normalized displacement plots shown in Fig. 13. Experiments with different initial water contents and the external voltages are also included in the figure. Similar to the observations made on the electric current, the higher initial water content or applied voltage results in larger displacements relaxing at a rate inversely proportional to the amount of water in the polymer.

Summary and Conclusions

A coupled model has been developed for the electromechanical response of polymeric membranes under an external

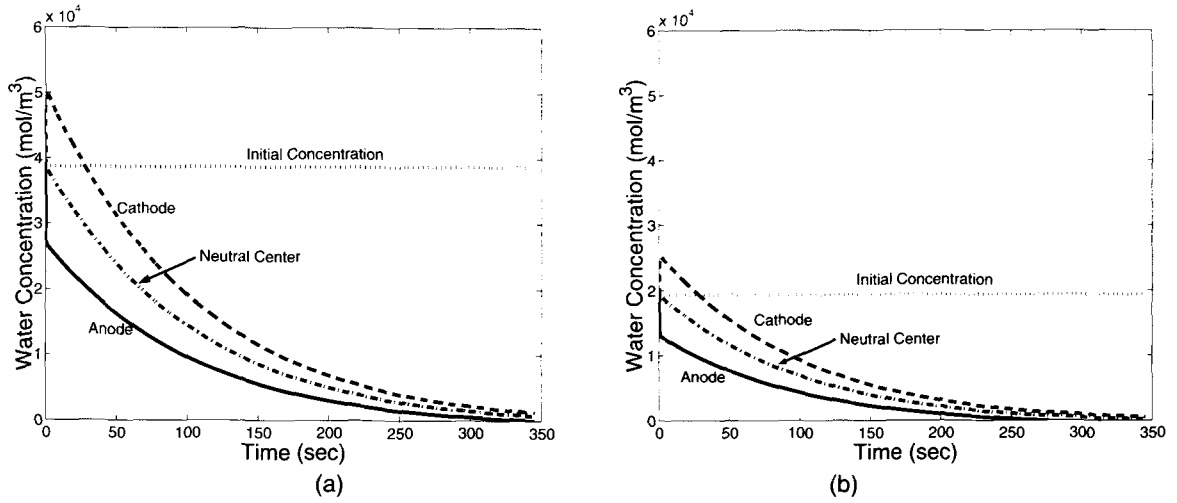

Fig. 9—History of water concentration during deformation of the fully (a) and 51% (b) hydrated IPMC actuators under an external voltage of 4 V

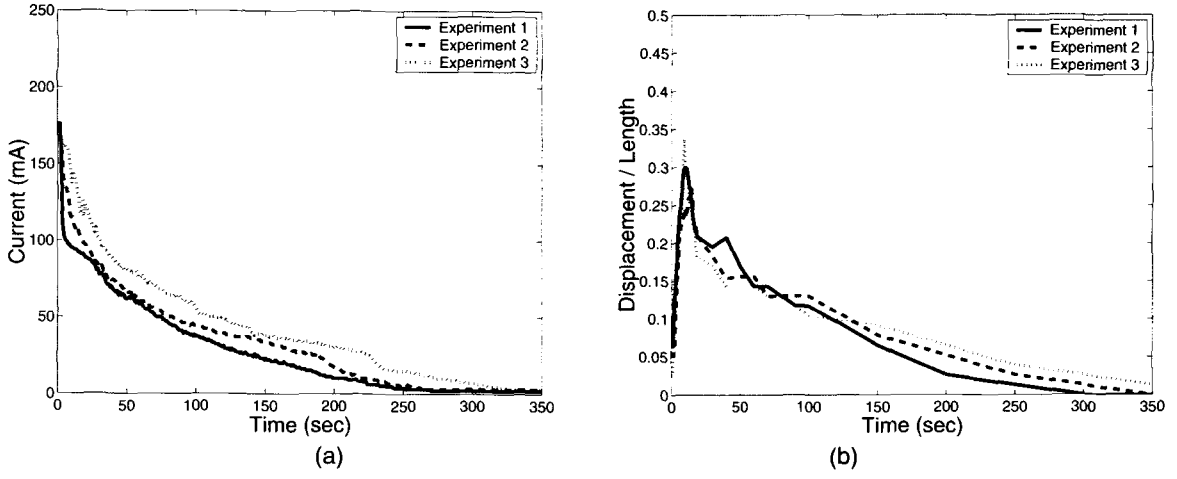

Fig. 10—The history of current (a) and displacement (b) of a fully hydrated IPMC actuator under an external voltage of 4 V

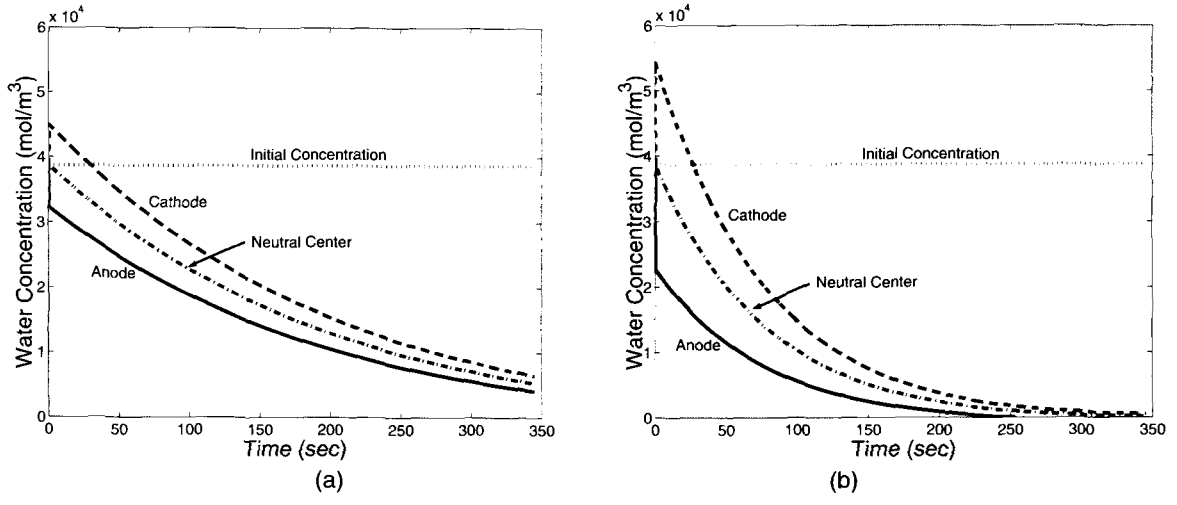

Fig. 11—History of water concentration during deformation of the fully hydrated IPMC actuators under external voltages of 3 V (a) and 5 V (b)

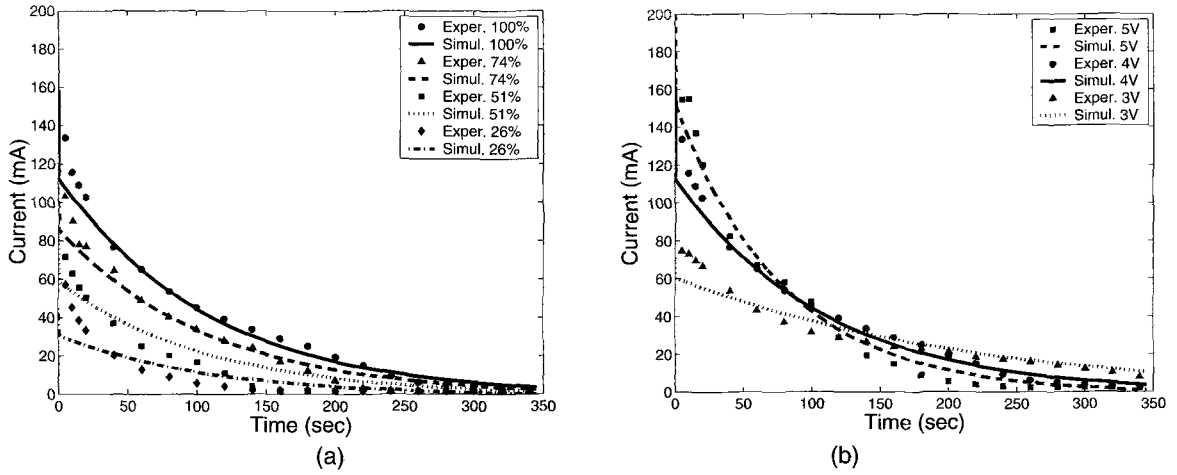

Fig. 12—Comparison of the history of current: the effect of initial water contents (a) and the effect of external voltages (b)

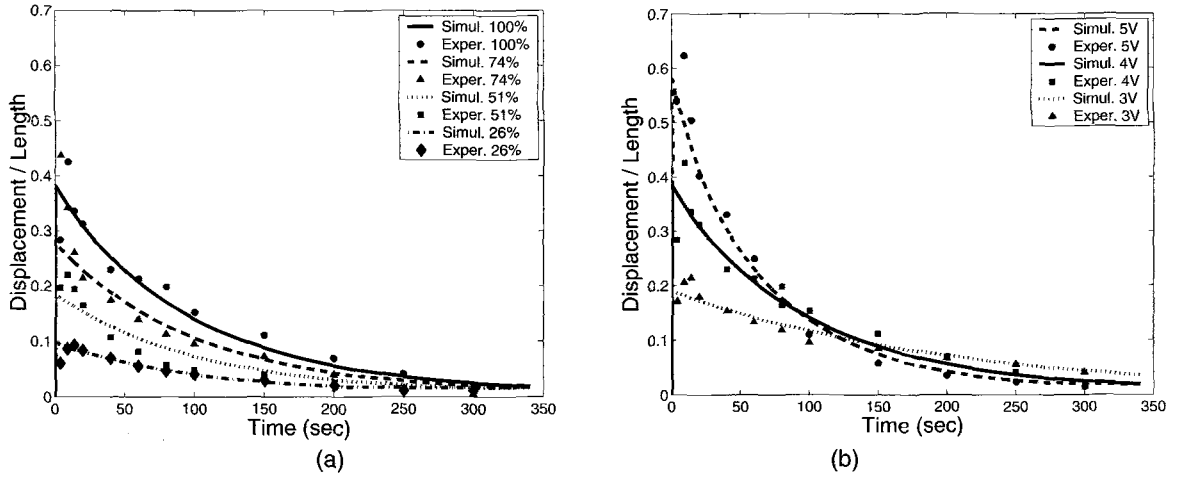

Fig. 13—Comparison of the history of displacement: the effect of initial water contents (a) and the effect of external voltages (b)

electric field. The fluxes in membrane were introduced using the Onsager thermodynamic theory, while the fluxes at both boundaries were derived from the reaction overpotential theory. The spatial gradients in the electrochemical potentials provided the driving force for mass transport across the bulk of the actuator. Through decomposition of the total strain into elastic and chemical strains, the model introduced explicitly the elastic strains into the chemical potential. The elastic behavior was modeled using a linear plane deformation model.

Comparison of simulation results based on independently determined transport coefficients with experimental data showed very good agreement between experimental and measured current and deformation history. Further, the observed currents and displacements were proportional to the initial water content and the externally applied voltage underlying the central role of water in the transport and deformation of these actuators when subjected to external potentials above the electrode equilibrium potentials.

The noticed deviation between simulation and experimental data during the initial 20 s of the experiment are most likely due to charging of the electrode interfaces,[16] which was not considered in this model.

The good agreement between experiments and simulations based on independent parameters seems to indirectly confirm the central role of water and its transport in the deformation process, as has been stipulated by others.[13,27,28] The proposed model does not appear to be in contradiction with other models dealing with the low-voltage regime, where short-lived and smaller-amplitude deflection can be expected due to electrostatic charging of the electrode regions as investigated by Nemat-Nasser and Li[5] and Nemat-Nasser.[14]

Acknowledgments

This research was supported in part by the National Science Foundation, grant number DMI-0134585.

References

1. Heitner-Wirguin, C., "Recent Advances in Perfluorinated Ionomer Membranes: Structure, Properties and Applications," Journal of Membrane Science, **120**, *1–33 (1996).*

2. Liu, R., Her, W-H., and Fedkiw, P.S., "In Situ Electrode Formation on a Nafion Membrane by Chemical Platinization," Journal of the Electrochemical Society, **139** (1), 15–23 (1990).

3. Oguro, K., Preparation Procedure Ion-Exchange Polymer Metal Composites (IPMC) Membranes, http://ndeaa.jpl.nasa.gov/nasa-nde/lommas/eap/IPMC_PrepProcedure.htm

4. Oguro, K., Fujiwara, N., Asaka, K., Onishi, K., and Sewa, S., "Polymer Electrolyte Actuator With Gold Electrodes," Proceedings of the SPIE, **3669**, 64–71 (1999).

5. Nemat-Nasser, S. and Li, J.Y., "Electrochemical Response of Ionic Polymer–metal Composites," Journal of Applied Physics, **87**(7), 3321–3331 (2000).

6. Nemat-Nasser, S. and Wu, Y., "Comparative Experimental Study of Ionic Polymer–metal Composites With Different Backbone Ionomers and in Various Cation Forms," Journal of Applied Physics, **93**, 5255–5267 (2003).

7. Shahinpoor, M., Bar-Cohen, Y., Simpson, J., and Smith, J., "Ionic Polymer–metal Composites (IPMCs) as Biomimetic Sensors, Actuators and Artificial Muscles: A Review," Smart Materials and Structures, **7**, R15–R30 (1998).

8. Jung, J., Kim, B., Tak, Y., and Park, J-O., "Undulatory Tadpole Robot (TadRob) Using Ionic Polymer–metal Composite (IPMC) Actuator," Proceedings of the 2003 IEEE/RSJ International Conference on Intelligent Robots and Systems, Las Vegas, NV, October, 2133–2138 (2003).

9. Shahinpoor, M., "Non-homogeneous Large Deformation Theory of Ionic Polymeric Gels in Electric and Ph Fields," Conference on Smart Structures and Materials, Proceedings of SPIE, **1916**, 40–50 (1993).

10. Shahinpoor, M., "Electromechanics of Iono-electric Beams as Electrically Controllable Artificial Muscles," Conference on Electroactive Polymer Actuators and Devices, Proceedings of the SPIE, **3669**, 109–121 (1999).

11. Kanno, R., Kurata, A., Hattori, M., Tadokoro, S., and Takamori, T., "Characteristics and Modeling of ICPF Actuator," Proceedings of the Japan–USA Symposium on Flexible Automation, Kobe, Japan, Vol. 2, 691–698 (1994).

12. Kanno, R., Tadokoro, S., Takamori, T., and Hattori, M., "Linear Approximate Dynamic Model of Ionic Conducting Polymer Gel Film Actuator," Proceedings of the IEEE International Conference on Robotics and Automation, Minneapolis, MN, Vol. 1, 219–225 (1996).

13. Bao, X., Bar-Cohen, Y., and Lih, S., "Measurements and Macro Models of Ionomeric Polymer–metal Composites (IPMCs)," Smart Structures and Materials Symposium, EAPAD Conference, San Diego, CA, Proc. of SPIE, **4695**, 220–227 (2002).

14. Nemat-Nasser, S., "Micromechanics of Actuation of Ionic Polymer–metal Composites," Journal of Applied Physics, **92**(5), 2899–2915 (2002).

15. Bockris, J. and Srinivasan, S., editors, Fuel Cells: Their Electrochemistry, McGraw-Hill, New York (1969).

16. Leary, S. and Bar-Cohen, Y., "Electrical Impedance of Ionic Polymeric Metal Composites," Proceedings of the SPIE 6th Annual International Symposium on Smart Structures and Materials, Newport Beach, CA, March 1–5, Paper No. 3669-09 (1999).

17. Hassanizadeh, S.M., "Derivation of Basic Equations of Mass Transport in Porous Media, Part 2. Generalizaed Darcy's and Fick's Laws," Advances in Water Resources, **9**, 207–222 (1986).

18. Enikov, E. and Boyd, J., "A Thermodynamic Field Theory for Anodic Bonding of Microelectromechanical Systems (MEMS)," International Journal of Engineering Science, **38**, 135–158 (2000).

19. Pourcelly, G., Lindheimer, A., Gavach, C., and Hurwitz, H., "Electrical Transport of Sulphuric Acid and in Nafion Perfluorosulphonic Membranes," Journal of Electroanalytical Chemistry, **305**, 97–113 (1991).

20. Vetter, K.J., Electrochemical Kinetics, Academic, New York (1967).

21. Moore, R.M., Fuel Cell Fundamentals, UC Davis (2003).

22. Daniels, F., Outlines of Physical Chemistry, Wiley, New York (1948).

23. Fales, J. and Vandeborough, N., "The Influence of Ionomer Channel Geometry on Ionomer Transport," Electrochemical Society Proceedings, **86**, 179–191 (1986).

24. Springer, T., Zawodzinski, T., and Gottesfeld, S., "Polymer Electrolyte Fuel Cell Model," Journal of the Electrochemical Society, **138** (1991).

25. West, A. and Fuller, T., "Influence of Rib Spacing in Proton-exchange Membrane Electrode Assemblies," Journal of Applied Electrochemistry, **26**, 557–565 (1996).

26. DuPont, Product Information: Nafion™ PFSA Membranes Perfluorosulfonic Acid Polymer, DuPont Fluoroproducts (2002).

27. Asaka, K. and Oguro, K., "Bending of Polyelectrolyte Membrane Platinum Composites by Electric Stimuli Part II. Response Kinetics," Journal of Electroanalytical Chemistry, **480**, 186–198 (2000).

28. Shahinpoor, M. and Kim, K., "Ionic Polymer–metal Composite: I. Fundamentals," Smart Materials and Structures, **10**, 819–833 (2001).